

# Assessment of 3D strength criteria of sand in the presence of strain localization

Madhu Sudan Negi<sup>1</sup>, S V Dharani Raj<sup>2</sup>, and Mousumi Mukherjee<sup>1,\*</sup>

<sup>1</sup>School of Civil and Environmental Engineering, Indian Institute of Technology, Mandi, 175005 Mandi, India

<sup>2</sup>School of Architecture and Civil Engineering, The University of Adelaide, 5005 Adelaide, Australia

**Abstract.** There exist various 3D strength criteria for sand that have been reported to accurately predict its strength response under homogeneous deformation conditions. However, the efficacy of these failure criteria in predicting strength under non-homogeneous deformation conditions, like in the presence of strain localization, has not been explored in detail. In the present study, a series of DEM based true triaxial simulations have been performed to investigate the influence of strain localization on the strength prediction by four commonly adopted 3D strength criteria for sand, i.e. Lade (1977), Ogawa (1974), Matsuoka-Nakai (1978) and Satake (1975) model. From the true triaxial simulations, it has been observed that strain localization in the form of a shear band develops within all the specimens when sheared under  $b > 0$  condition, where  $b$  is the intermediate principal stress ratio. Among the adopted strength criteria, the Lade criterion estimates comparable peak stresses with reference to the DEM results. However, due to the formation of persistent shear bands, all four models significantly overpredict the strength response at the critical state. Additionally, at the critical state, the stresses within the shear band region have been noticed to converge at a local  $b$  value between 0.2 – 0.4 and become independent of the applied global  $b$  value.

## 1 Introduction

Soil elements in various geotechnical structures are often subjected to loading conditions with unequal principal stresses in three directions i.e.,  $\sigma_1 \neq \sigma_2 \neq \sigma_3$ , where  $\sigma_1$ ,  $\sigma_2$  and  $\sigma_3$  are the major, intermediate and minor principal stress, respectively. Various experimental studies based on the true triaxial and hollow cylinder tests have also reported a strong dependence of the shear strength of soil on the intermediate principal stress [1,2]. These insights have led to the development of several 3D strength criteria that can account for such intermediate principal stress dependency [3–6]. These failure criteria have been reported to accurately predict the strength response of geomaterials under homogeneous deformation conditions. However, in the case of the occurrence of strain localization, i.e. non-homogeneous deformation within the specimen, the prediction of these failure criteria has not been explored in detail. Such strain localization in the form of shear bands often emerges in sand under real field conditions like slope failures, retaining walls and foundations etc. Hence, assessing the prediction of these 3D failure criteria in the presence of strain localization becomes imperative for the accurate modeling of such boundary value problems.

The strength estimation of four commonly adopted 3D strength criteria has been assessed here based on the results obtained from the 3D Discrete Element Method (DEM) based simulations of true triaxial test [7]. Particular focus has been given to the stress states prevailing inside and outside the shear band region, and the strength prediction of the chosen strength criteria has been analyzed separately for these stress states.

## 2 True triaxial test simulation

In the present study, 3D DEM simulations of true triaxial test have been carried out employing PFC 3D. The simulation results have been validated against the true-triaxial experimental data reported by Wang and Lade [1] on Santa Monica beach sand. Following the test configuration, a cuboidal specimen of 76 mm  $\times$  76 mm  $\times$  188 mm with rigid frictionless walls has been generated containing spherical particles of size distribution (PSD) as depicted in Fig 1. For reducing the computational time, the PSD has been up-scaled by 6 times of the actual PSD used in the experiments, leading to the generation of approximately 0.63 million spherical particles for an initial porosity of 0.4 [8]. The relative density (RD = 90 %) of the simulated assembly has been matched with the experimental data. Further, a density scaling of 1000 has also been adopted in the DEM simulation to aid the computation time [9].

DEM simulations of drained true triaxial test have been conducted on the dense sand specimen with various intermediate principal stress ratios,  $b = (\sigma_2 - \sigma_3)/(\sigma_1 - \sigma_3)$ . During shearing, a constant confining pressure of  $\sigma_3 = 49$  kPa has been maintained on one set of vertical walls, and the stresses on the other set of vertical walls have been adjusted by employing the servo mechanism to maintain a constant stress condition as per the desired  $b$  value. The top and bottom walls are moved at an axial strain rate of  $\dot{\epsilon}_1 = 0.01/s$  while ensuring the quasistatic conditions. A linear rolling resistance contact model has been employed in the present study, which can indirectly account for the rotational resistance arising due to angular sand particles

\* Corresponding author: [mousumi@iitmandi.ac.in](mailto:mousumi@iitmandi.ac.in); [mousumi.ju06@gmail.com](mailto:mousumi.ju06@gmail.com)

[10]. The micromechanical parameters used for the DEM simulations are listed in Table 1, which has been obtained after an iterative calibration procedure to match the macro level experimental results of Wang and Lade [1].

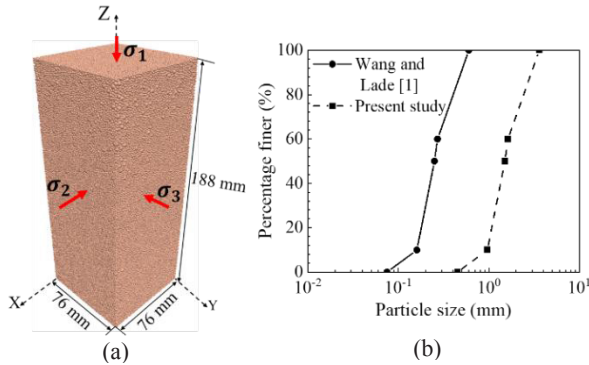


Fig. 1. (a) Schematic representation of the triaxial test and (b) particle size distribution curve.

Table 1. Calibrated micromechanical parameters.

Parameters	Values
Particle density, $\rho$	$2660 \times 10^3 \text{ kg/m}^3$
Effective normal contact stiffness, $E$	600 MPa
Normal to shear stiffness ratio, $k$	10
Sliding friction coefficient, $\mu_s$	0.48
Rolling resistance coefficient, $\mu_r$	0.9

### 3 Strength prediction

An assessment of the strength predictions by the four commonly adopted 3D failure criteria i.e., Lade (1977) [3], Ogawa (1974) [4], Matsuoka-Nakai (1978) [5] and Satake (1975) [6] has been carried out with reference to the simulated true triaxial test results. These failure criteria have been chosen in the present study as they consider the intermediate principal stress into the formulation. The expressions for the Lade, Ogawa, Matsuoka-Nakai and Satake models have been given in Equations 1, 2, 3 and 4, respectively.

$$\eta_L = \left( \frac{I_1^3}{I_3} - 27 \right) \left( \frac{I_1}{p_a} \right)^m \quad (1)$$

$$\eta_O = \left( \frac{I_2}{I_1^2} \right) + n \left( \frac{3I_3 - I_2 I_1}{3I_1^3} \right) \quad (2)$$

$$\eta_{MN} = \left( \frac{\sigma_1 - \sigma_3}{\sigma_1 \sigma_3} \right)^2 + \left( \frac{\sigma_1 - \sigma_2}{\sigma_1 \sigma_2} \right)^2 + \left( \frac{\sigma_2 - \sigma_3}{\sigma_2 \sigma_3} \right)^2 \quad (3)$$

$$\eta_S = \left( \frac{\sigma_1 - \sigma_3}{\sigma_1 + \sigma_3} \right)^2 + \left( \frac{\sigma_1 - \sigma_2}{\sigma_1 + \sigma_2} \right)^2 + \left( \frac{\sigma_2 - \sigma_3}{\sigma_2 + \sigma_3} \right)^2 \quad (4)$$

Both the Lade and Ogawa models incorporate two parameters ( $\eta_L$  &  $m$  for Lade and  $\eta_O$  &  $n$  for Ogawa); whereas, the Matsuoka-Nakai and Satake models use a single parameter ( $\eta_{MN}$  for Matsuoka-Nakai and  $\eta_S$  for Satake) to represent the failure envelope. Further,  $p_a$  is the atmospheric pressure, which has been taken as 101.325 kPa and  $I_1$ ,  $I_2$  and  $I_3$  are the invariants of the stress tensor.

The parameters for the adopted failure criteria have been summarized in Table 2, which have been obtained by fitting the corresponding equations against the

obtained true triaxial stresses at peak and critical state. The peak state is marked when the granular assembly attains a maximum deviatoric stress; whereas, the critical state indicates a state of continuous deformation without any changes in the stresses state or volume of the granular assembly.

Further, the failure envelope predicted from the 3D strength criteria has been compared with the simulated true triaxial stress states in the deviatoric plane ( $\pi$  plane) and also in reference to the estimated 2D friction angle i.e.,  $\phi = \sin^{-1}[(\sigma_1 - \sigma_3)/(\sigma_1 + \sigma_3)]$ , which are depicted in Figure 2 at the peak stress state. It can be observed that all the adopted 3D failure criteria predict the exact strength response of the specimen for the triaxial compression ( $b = 0$ ) condition. The two parameter models, i.e. Ogawa and Lade, overpredict the peak stresses particularly in the mid-range of  $b$  values; whereas, the single parameter models, i.e., Matsuoka-Nakai and Satake underpredict the peak stresses at higher  $b$  values. Both the single parameter models estimate almost similar peak stresses for all the  $b$  values, with a slight deviation for  $b$  values of 0.2 – 0.4. Further, it can be noted that the single parameter models predict almost similar stresses for the triaxial compression ( $b = 0$ ) and extension ( $b = 1$ ) conditions. However, the two parameter models predict higher stresses for the extension condition as compared to the compression condition. Overall, the Lade model estimates almost similar peak strength response as obtained from the DEM simulations, particularly for the range,  $b \leq 0.2$  and  $b \geq 0.8$ . However, a significant overestimation by the Lade failure criterion for the mid-range values of  $b$ , i.e.  $0.2 < b < 0.8$ .

From the true triaxial simulations, it has been observed that strain localization in the form of a single shear band emerges extending from one corner of the specimen to its diagonally opposite corner when subjected to shearing with  $b > 0$ . On the contrary, a homogeneous deformation field without any distinct shear band is evident when sheared under the triaxial compression condition ( $b = 0$ ). Furthermore, for the mid-range values of  $b$ , i.e.  $0.2 < b < 0.8$ , such bands emerge in the hardening regime. As a result, the mobilized shear strength of the specimen might be lower than the strength that would have been achieved in the absence of any band formation, which is indicated by the overpredicted shear strength by the Lade's criterion for these mid-range values of  $b$ .

Table 2. Fitted parameters for the adopted failure criteria.

Failure criteria	Peak state	Critical state
Lade	$\eta_L = 20.75$ $m = 0.2$	$\eta_L = 14.4$ $m = 0.15$
Ogawa	$\eta_O = 0.0697$ $n = 2.565$	$\eta_O = 0.07$ $n = 2.825$
Matsuoka-Nakai	$\eta_{MN} = 6.44$	$\eta_{MN} = 4.15$
Satake	$\eta_S = 0.893$	$\eta_S = 0.685$

A similar strength comparison at the critical state has been depicted in Fig. 3. Owing to the formation of the persistent (fully developed) shear band, the overall stresses at the critical state reduce significantly within

the specimens when sheared under  $b > 0$  conditions. Hence, all the adopted failure criteria overpredict the overall strength response of the specimen at the critical state for conditions  $b > 0$ , where the shear band forms within the specimen. Additionally, it can be noticed from Fig. 3(b) that the critical state friction angle is nearly constant between  $32^\circ$  to  $34^\circ$  for all these cases where the shear band develops, regardless of the  $b$  value.

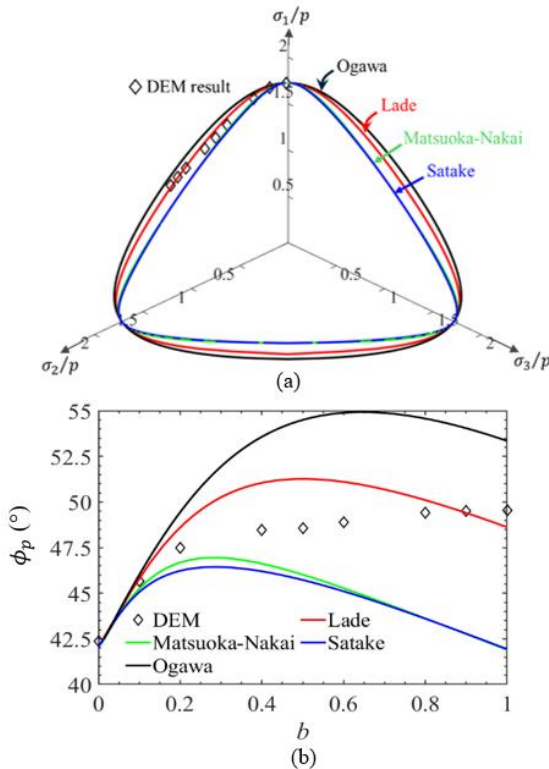


Fig. 2. Comparison of the peak strength estimation by the adopted strength criteria (a) in  $\pi$  plane, and (b) in terms of 2D friction angle.

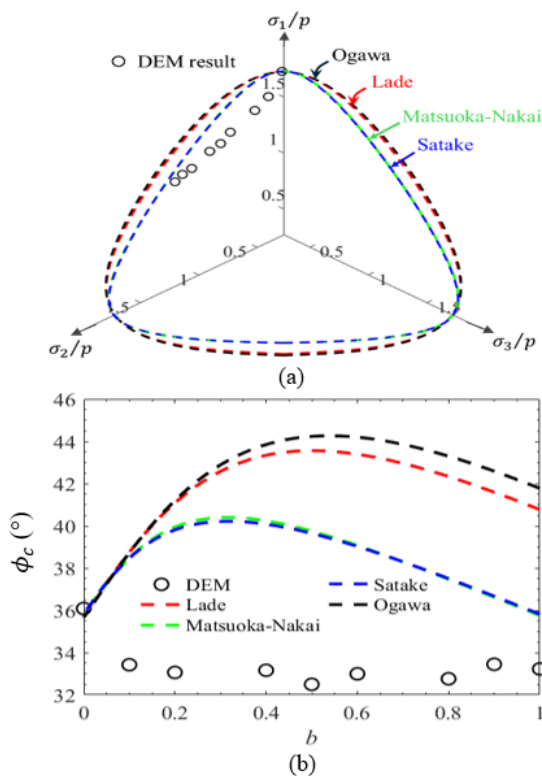


Fig. 3. Comparison of the strength estimation by the adopted strength criteria at the critical state (a) in  $\pi$  plane, and (b) in terms of 2D friction angle.

### 4 Influence of strain localization

In order to further understand the influence of strain localization on the strength estimation, the stresses from both inside and outside of the shear band region have been estimated along with the overall stress state of the specimen, and further compared against the already fitted 3D failure surfaces. The stresses inside and outside of the shear band region have been estimated based on the volume averaged stresses obtained from the measurement spheres (representative volume elements) of diameter equal to 12 times  $d_{50}$  of particles as depicted in Fig. 4(a). The evolution of stress ratio ( $q/p$ ) inside and outside the shear band region during shearing under  $b = 0.2$  condition has been shown in Fig. 4(b). It can be observed that the stresses inside the shear band region are significantly lower as compared to the stresses outside the shear band region. This is due to the buckling of elongated strong force chains within the shear band region, which, reduces the stresses within the shear band [10,11].

Further, the stresses inside and outside the shear band at both the peak and the critical state have been compared with the earlier fitted failure envelopes corresponding to the Lade and Matsuoka-Nakai model as depicted in Fig. 5. It can be observed that the stresses outside the shear band region are higher than the same noted inside the shear band at both the peak and critical state for shearing under  $b > 0$  conditions. It is also interesting to note that after the full development of the shear band i.e., at the critical state, the stress state within the shear band becomes independent of the applied global stress conditions and converges to a  $b$  value between 0.2 – 0.4, which usually corresponds to the plane strain condition [12] [Fig. 5(b)].

This difference in the stress state inside and outside the shear band indicates the importance of considering a two-scale continuum framework, where the region outside and inside the localized zone can be considered separately based on an internal length scale parameter that depends on the thickness of the shear band [13].

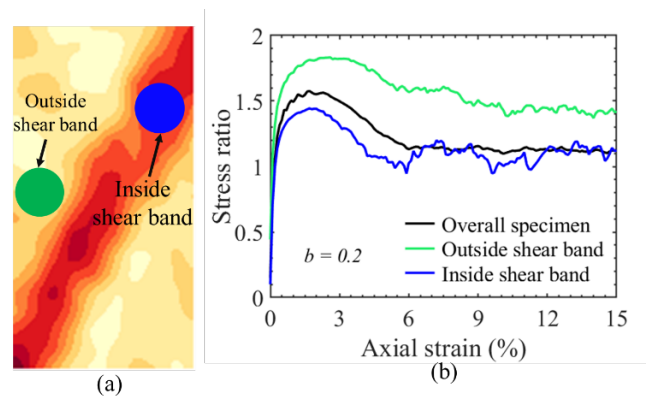
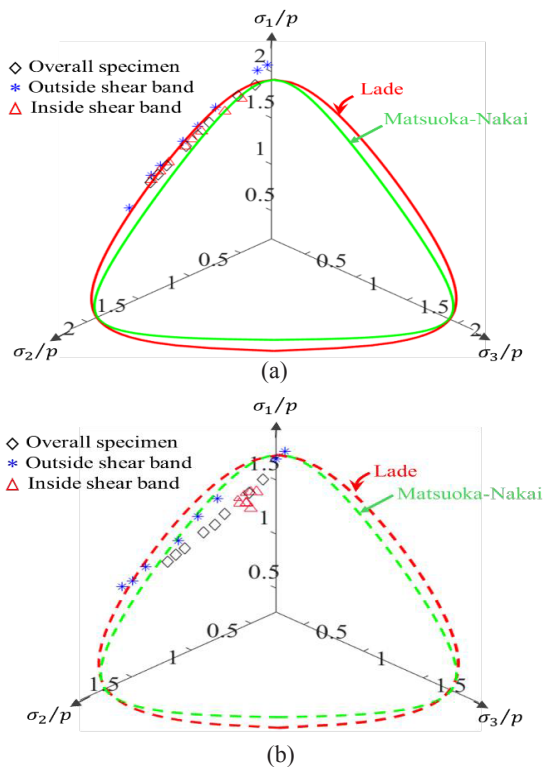


Fig. 4. (a) Position of measurement sphere inside and outside the shear band region, (b) evolution of stress ratio ( $q/p$ ) inside and outside shear band during shearing under  $b = 0.2$  condition.



**Fig. 5.** Comparison of stresses inside and outside shear band region along with the global stress estimation in  $\pi$  plane (a) at peak stress, and (b) at critical state.

## 5 Conclusions

In the present study, DEM based true triaxial simulations have been performed with varying  $b$  values. The strength estimation has been carried out employing four commonly adopted 3D strength criteria in reference to the simulated true triaxial test results. The adopted failure criteria have been assessed by comparing the failure envelopes predicted from these strength criteria against the simulated true triaxial stress state in the  $\pi$  plane and also in reference to the estimated 2D friction angle at both peak and critical state. Further, in order to assess the influence of strain localization on the strength estimation, along with the overall stress of the specimen, the stress states from both the inside and outside of the shear band region have been considered and further compared against the predictions from these 3D failure criteria.

It has been observed that compared to the other adopted 3D strength criteria, the Lade model estimates a very comparable peak strength response in reference to the DEM simulated data, particularly for  $b \leq 0.2$  and  $b \geq 0.8$ . However, a significant overestimation in the peak strength estimation has been observed for the mid-range values of  $b$ , i.e.  $0.2 < b < 0.8$ . This overestimation in the peak strength is due to the formation of the shear band within the specimen at the hardening regime when subjected to shearing under these mid-range  $b$  values. However, at the critical state, due to the development of the persistent shear band, all the adopted failure criteria overpredict the overall strength of the specimen when the shearing is performed under  $b > 0$  condition. Additionally, it has been noted that, at the critical state,

the stress state within the shear band becomes independent of the applied global stress conditions and converges to a  $b$  value between 0.2 – 0.4, which usually corresponds to the plane strain conditions.

The authors would like to acknowledge the support rendered by Dr. Arghya Das from Indian Institute of Technology Kanpur, India for granting access to the PFC 3D software.

## References

1. Q. Wang, P. V. Lade, Shear banding in true triaxial tests and its effect on failure in sand, *J. Eng. Mech.* **127**, 754–761 (2001).
2. R.K. Kandasami, T.G. Murthy, Experimental studies on the influence of intermediate principal stress and inclination on the mechanical behaviour of angular sands, *Granul. Matter* **17**, 217–230 (2015).
3. P. V. Lade, Elasto-plastic stress-strain theory for cohesionless soil with curved yield surfaces, *Int. J. Solids. Struct.* **13**, 1019–1035 (1977).
4. S. Ogawa, S. Mitsui, O. Takemure, Influence of the intermediate principal stress on mechanical properties of a sand, in *Proceedings of 29th Annual meeting of Japan Society of Civil Engineering*, Tokyo, Japan, 49–50 (1974).
5. H. Matsuoka, T. Nakai, A generalized frictional law for soil shear deformation. In *Proceedings of the US-Japan seminar on continuum-mechanical and statistical approaches in the mechanics of granular materials*, Tokyo, Japan, 138–154 (1978).
6. M. Satake, Consideration of yield criteria from the concept of metric space, *The Technology reports of Tohoku University* **40**, 230–524 (1975).
7. P.A. Cundall, O.D.L. Strack, A discrete numerical model for granular assemblies, *Geotechnique*, **29**, 47–65 (1979).
8. X. Lü, Y. Ma, J. Qian, M. Huang, Discrete-Element Simulation of Scaling Effect of Strain Localization in Dense Granular Materials, *Int. J. Geomech.* **19**, 1–10 (2019).
9. C. Thornton, Numerical simulations of deviatoric shear deformation of granular media, *Geotechnique*, **50**, 43–53 (2000).
10. M. Iwashita K., Oda, Rolling resistance at contacts in simulation of shear band, *J. Eng. Mech.* **124**, 285–292 (1998).
11. M.S. Negi, M. Mukherjee, Effect of confining stress and lateral boundary conditions on the drained instability response of sand: a DEM based assessment across the length scales, *Granul. Matter* **27** (2025).
12. P. Anantanasakul, J.A. Yamamuro, P. V. Lade, Three-dimensional drained behavior of normally consolidated anisotropic kaolin clay, *Soils Found.* **52**, 146–159 (2012).
13. G. D. Nguyen, I. Einav, and A. M. Korsunsky. How to connect two scales of behaviour in constitutive modelling of geomaterials. *Geotechnique Letters*, **2(3)**, 129–134 (2012).